

Surface Kuroshio Intrusion Evidenced by Satellite Geostrophic Streamlines: Algorithm and Seasonal variations

Yisen Zhong¹, Meng Zhou¹, Joanna Jadwiga Waniek², Lei Zhou¹, and Zhaoru Zhang¹

¹Shanghai Jiao Tong University

²Institute for Baltic Sea Research Warnemünde

November 22, 2022

Abstract

Using long-term satellite altimeter data, a new streamline-based algorithm is developed to identify the Kuroshio intrusion types and describe the seasonal variations of related dynamical properties. Results from this new classification show that a mixing of leaping, looping and leaking streamlines is the dominant form of Kuroshio intrusion into the South China Sea (SCS). The leaping path is very stable and crosses the Luzon Strait mainly through the Balintang Channel regardless of seasons, while the streamlines leaking into the SCS is more likely to intrude via the channel between the Babuyan Island and the Camiguin Island. Large seasonal variations are found with the percentage of each kind of streamline and the Luzon Strait Transport (LST), but not with the intensity, width and current axis position of the Kuroshio. The along-streamline analysis reveals that the seasonal intrusion of the Kuroshio is essentially the seasonal variation of the cyclonic shear part of the flow. A possible physical mechanism is proposed to accommodate these seasonal characteristics based on globally the vorticity (torque work) balance between the basin-wide wind stress and the lateral friction, as well as locally the loss of balance between the torques of interior stresses and normal stresses both provided by the wall boundary, together with a plausible conjecture that the seasonally-reversing monsoon can significantly modify the torque of the interior stresses within the cyclonic shear part of the flow and thus responsible for the seasonal variation of the Kuroshio intrusion.

1 **Surface Kuroshio Intrusion Evidenced by Satellite Geostrophic**

2 **Streamlines: Algorithm and Seasonal variations**

3 **Yisen Zhong¹, Meng Zhou¹, Joanna J. Waniek², Lei Zhou^{1,3}, Zhaoru Zhang¹**

4 ¹School of Oceanography, Shanghai Jiao Tong University, Shanghai, China, ²Leibniz
5 Institute for Baltic Sea Research Warnemünde, Seestraße 15, 18119 Rostock,
6 Germany, ³Southern Marine Science and Engineering Guangdong Laboratory
7 (Zhuhai), Zhuhai, China.

8 Email: yisen.zhong@sjtu.edu.cn; meng.zhou@sjtu.edu.cn

9 **Abstract**

10 Using long-term satellite altimeter data, a new streamline-based algorithm is
11 developed to identify the Kuroshio intrusion types and describe the seasonal
12 variations of related dynamical properties. Results from this new classification show
13 that a mixing of leaping, looping and leaking streamlines is the dominant form of
14 Kuroshio intrusion into the South China Sea (SCS). The leaping path is very stable
15 and crosses the Luzon Strait mainly through the Balintang Channel regardless of
16 seasons, while the streamlines leaking into the SCS is more likely to intrude via the
17 channel between the Babuyan Island and Camiguin Island. Large seasonal variations
18 are found with the percentage of each kind of streamline and the Luzon Strait
19 Transport (LST), but not with the intensity, width and current axis position of the
20 Kuroshio. The along-streamline analysis reveals that the seasonal intrusion of the
21 Kuroshio is essentially the seasonal variation of the cyclonic shear part of the flow. A
22 possible physical mechanism is proposed to accommodate these seasonal
23 characteristics based on globally the vorticity (torque work) balance between the
24 basin-wide wind stress and the lateral friction, as well as locally the loss of balance
25 between the torques of interior stresses and normal stresses both provided by the wall
26 boundary, together with a plausible conjecture that the seasonally-reversing monsoon

27 can significantly modify the torque of the interior stresses within the cyclonic part of
28 the flow and thus responsible for the seasonal variation of the Kuroshio intrusion.

29 **Plain Language Summary**

30 The Kuroshio Current, when flowing past the Luzon Strait, has a tendency of
31 meandering into the Strait. The meandering current bifurcates with a branch into the
32 South China Sea more frequently in winter than in summer. The reason why the
33 Kuroshio intrusion varies seasonally remains unclear. In this study, a new
34 streamline-based algorithm is developed, which facilitates us to investigate this
35 problem with the long-term satellite data. We found that the Kuroshio width, intensity
36 and position barely change within a seasonal cycle, and the intrusion branch is mainly
37 the cyclonic shear part of the Kuroshio. The finding of these characteristics makes us
38 look for a new interpretation for the seasonal intrusion. The global wind stress is
39 responsible for Kuroshio leaping across the Strait, and the unbalanced torque of the
40 lateral friction when the current loses contact with the wall tends to push the Kuroshio
41 into the South China Sea. The strength of the unbalanced torque may be significantly
42 modified by the seasonally-reversing monsoon. The combined effects explain the
43 seasonal variability of the Kuroshio intrusion.

44 **1. Introduction**

45 The Kuroshio intrusion into the South China Sea (SCS) has been a long debate
46 for decades (see the review paper by Nan et al., 2015). The warm and salty Kuroshio
47 flows northwards along the eastern coast of Philippine. When encountering a
48 boundary gap, Luzon Strait (LS) in this case, the current can either leap across the gap
49 or bifurcates with a branch through the LS in the form of a loop current or a direct
50 intrusion. The water enters the SCS mainly via the Balintang Channel and most of
51 them subsequently exits through the Bashi Channel (Liang et al., 2008; Yuan et al.,
52 2008). But the intrusion can efficiently exchange the momentum, heat and other
53 tracers between the SCS and the Pacific (Nan et al., 2015; Qu et al., 2004; Wu, 2013;

54 Xu & Su, 2000).

55 To investigate the Kuroshio intrusion mechanism, the first step is usually to find
56 a way to describe the Kuroshio intrusion paths and their variation in time. Previous
57 methods almost always use the indirect parameters to indicate the variation of the
58 intrusion such as an areal integral of geostrophic vorticity over the intrusion paths
59 southwest of Taiwan (Nan et al., 2011a), the mean pressure (sea level anomaly) in a
60 certain region west of the LS (Wu, 2013) etc. These parameters are indeed successful
61 in interpreting many important findings on the intrusion characteristics on various
62 time scales (Nan et al., 2015; Chen et al., 2020). However, the correlation between
63 these parameters and the climate variables is usually not satisfactorily high, e.g. a
64 correlation of 0.53 between Pacific Decadal Oscillation (PDO) index and interannual
65 variability of intrusion shown in Wu (2013). The moderate correlation could be due to
66 incompetent representation of intrusion with a single dynamical factor. Another issue
67 with the traditional methods is that they typically categorize Kuroshio intrusion into
68 three to five types using a subjectively determined threshold, but disregard the
69 continual transition among different intrusion types. In other words, the variations of
70 the strength of each intrusion type are not fully considered. This information may be
71 essential for studying the intrusion mechanism especially when relating it to the
72 variation of external forcing.

73 The Kuroshio intrusion has a strong seasonal cycle with more intrusion in winter
74 and less in summer evidenced by both observational and modelling results. For
75 decades a large volume of studies has been devoted to this topic (e.g. Farris &
76 Wimbush, 1996; Hsin et al., 2012; Lan et al., 2004; Qu, 2000; Xu et al., 2004; Yang et
77 al., 2013; Yaremchuk & Qu, 2004). However, the dynamical mechanism responsible
78 for this remains unclear. The common knowledge is that the Kuroshio is nearly
79 always bent into the LS but only a portion of the current can continue to move
80 westwards into the SCS. The process of Kuroshio intrusion into the SCS can then be
81 thought as a two-step problem. The first is what mechanism steers the Kuroshio into

82 the LS via different channels. Sheremet (2001) presents that the intrusion regime
83 depends on the Reynolds number, i.e. the larger the transport or the inertia is, the
84 more likely the flow leaps across the gap. He thus concludes that the Kuroshio
85 normally leaps across the LS and penetrates into the SCS only when its strength is
86 significantly reduced. The potential vorticity distribution is also found related to the
87 intruding angle, speed and path (Nan et al. 2015; Sheu et al., 2010; Xue et al. 2004).
88 Kuehl and Sheremet (2009) infer from the laboratory experiments that the Ekman
89 transport may affect the Kuroshio intrusion by slightly changing the inflow angle.

90 The second problem can be stated as what drives the intrusion branch goes
91 further into the SCS while not turns back to the path of the main stream, after the
92 current enters the LS. On the seasonal time scale, this part of intrusion is primarily
93 attributed to the local seasonally-reversing monsoon. Without the monsoon the upper
94 Luzon Strait Transport (LST) could change from westward to eastward with
95 misaligned seasonality (Hsin et al., 2012). Many previous studies show a close
96 relationship between the intrusion transport and the wind-driven Ekman transport
97 (Metzger & Hurlburt, 2001; Nan et al., 2001b), but the direct contribution of Ekman
98 transport accounts for less than 10% of the total LST (Qu et al., 2004). Wu and Hsin
99 (2012) show that the northwestward Ekman transport in winter can increase the
100 probability of intrusion into the SCS by accelerating the upstream Kuroshio in the LS.
101 They also point out that the existence of negative wind stress curl off the southwest
102 Taiwan is crucial to triggering the intrusion.

103 The conclusions for the above two problems in previous studies come mainly
104 from the laboratory or numerical experiments, owing to the lack of long-term in-situ
105 measurements. Hence supports and validations from observational evidence are still
106 needed. Currently only the satellite data can provide such a qualified tool to evaluate
107 the variability of the surface, despite only geostrophic, transports of Kuroshio
108 intrusion on various time scales. Song (2006) shows the (LST) is mainly geostrophic
109 in the upper 1500 m, suggesting that the geostrophic transports derived from satellite

110 data are adequate to represent the major intrusion, given that the direct Ekman effect
111 is proved to be small. In fact, various satellite products have been used to describe the
112 intrusion patterns in a more qualitative manner (e.g. Farris & Wimbush, 1996; Yuan et
113 al. 2006). In this study, we develop a new geometric method to both identify the
114 intrusion types and quantify the seasonal variation of related dynamical properties
115 using satellite altimetry data. A number of detailed but new findings are reported here
116 and a suitable mechanism that accommodates these findings is then sought to interpret
117 the seasonal variation of the Kuroshio intrusion.

118 **2. Data and Method**

119 **2.1 Satellite altimeter data**

120 The satellite data used here is the global ocean gridded L4 sea surface height
121 from 1993 to 2018 reprocessed by Copernicus Climate Service. This product is
122 suggested for studying ocean circulation and long-term variability because the
123 processing focuses on the stability and homogeneity of the sea level records based on
124 two-satellite constellation. Though multiple satellites can improve the spatial
125 sampling, the introduction of a new satellite could lead to some biases and thus impair
126 the data stability. The absolute dynamic height data is mapped onto a $0.25^\circ \times 0.25^\circ$
127 horizontal grid on a daily basis. As large biases may occur in the coastal region, the
128 altimeter data in regions with water depth less than 300 m are discarded.

129 **2.2 Streamline-based pattern recognition**

130 Here we propose a geometric algorithm to recognize the flow pattern of Kuroshio
131 intrusion into the SCS based on geostrophic streamlines derived from satellite
132 altimeter data. For the surface geostrophic flow, the isopleth of sea surface level is a
133 proxy of current streamline according to the geostrophic relation below.

$$u = -\frac{\partial\phi}{\partial y} = -\frac{g}{f}\frac{\partial\zeta}{\partial y}, \quad v = \frac{\partial\phi}{\partial x} = \frac{g}{f}\frac{\partial\zeta}{\partial x}, \quad \phi = \frac{g}{f}\zeta \#(1)$$

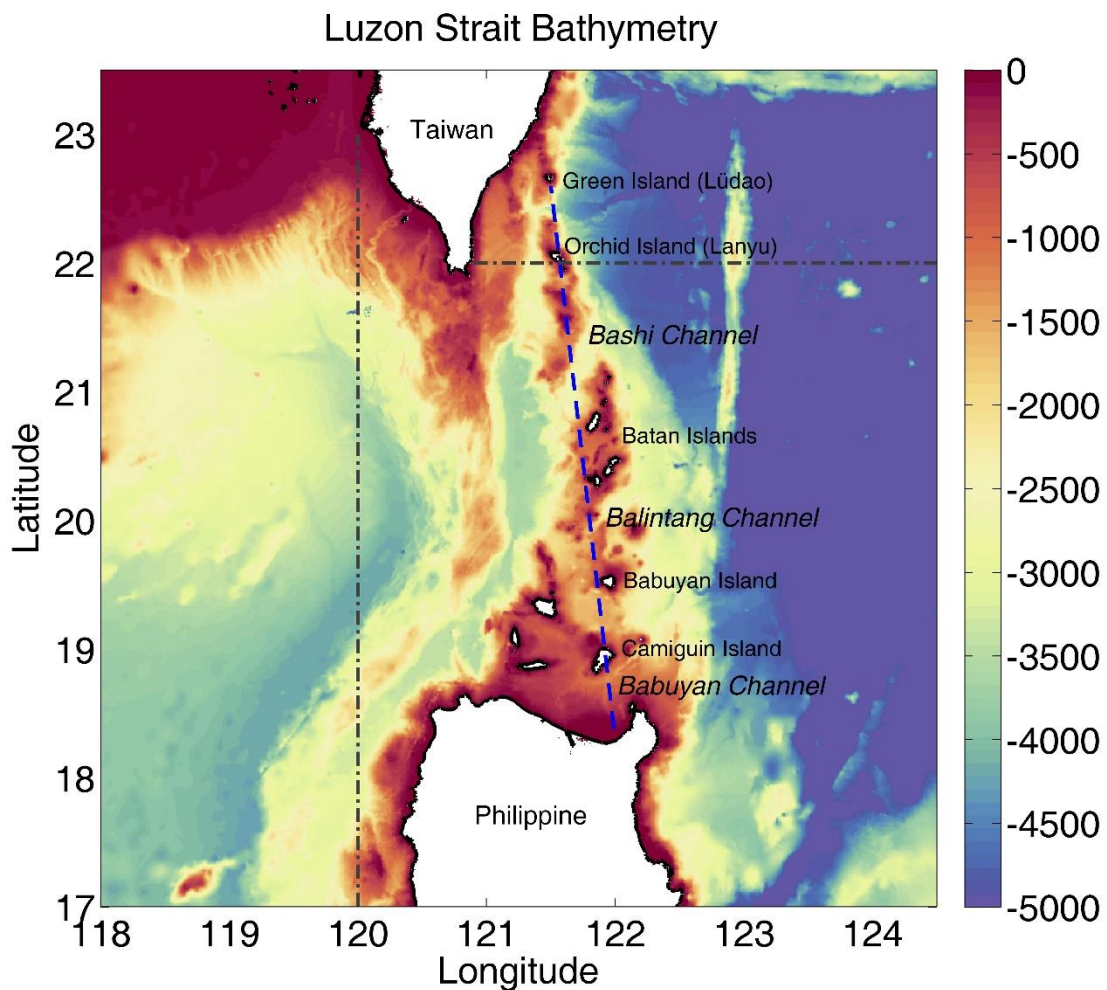
134 where ζ, u, v, ϕ are satellite sea surface elevation, longitudinal and latitudinal
135 geostrophic velocities and geostrophic stream function respectively. By tracking the
136 extension of streamlines originated from Kuroshio east of Philippine, different types
137 of Kuroshio intrusion can be easily distinguished.

138 The Kuroshio Current, when encountering the LS, may bypass the Strait and go
139 directly north, or take a detour to visit the SCS and then loop back to the main path, or
140 intrude into the SCS directly. However, not all the time does the entire Kuroshio
141 follow only one of the above routes. The current sometimes bifurcates with one
142 branch going one way and the other going another. The 3L classification (Leap:
143 bypassing, Loop: looping, Leak: bypassing and intruding, Nan et al. 2011a) describes
144 three typical combinations of the above routes. Here we might as well borrow these
145 three words to define the type for each Kuroshio streamline instead of the entire
146 current. The Leap and Loop keep their original meanings while the Leak represents
147 the streamlines that intrude the SCS. Each combination of these three kinds of
148 streamlines makes one Current intrusion type, so in theory there should be seven types
149 of current intrusion. As will be shown below, only four of them are important and the
150 rest are either nonexistent or very rare (Table 1). The Kuroshio Current Loop could
151 shed an eddy into the SCS from time to time. In this study we consider these eddies as
152 a “gift” left by the loop current but not part of the main stream, therefore we will not
153 categorize this type. Caruso et al. (2006) identifies a cyclonic loop intrusion type from
154 the satellite sea surface temperature and the sea level anomaly, which cannot be
155 distinguished by our algorithm as streamlines do not braid.

156 A series of criteria must be carefully defined to identify the above streamline
157 types. We select the streamlines that pass through a transect along the latitude 19°N
158 between 122°E and 124°E to represent the Kuroshio. This transect is located to the
159 northeast of Philippine, where the entire incoming flow can be well captured. The
160 west bound of the transect is located to the east of the Camiguin Island with water
161 depth over 300 m, and the east bound is determined to make the transect slightly

162 longer than the width of the Kuroshio Current. This choice would not affect the final
 163 results because only the streamlines belonging to the above-mentioned types will be
 164 accounted in the subsequent analysis. The streamlines passing this transect with
 165 spatial interval of 0.01 m (isopleths of sea level) are tracked in the domain of 16–
 166 26°N and 110–126°E. Using equally-spaced isopleths renders the streamline number
 167 to represent the surface geostrophic transport. The Leap, Loop and Leak streamlines
 168 are defined according to the following criteria (Figure 1).

- 169 ● If a streamline never intersects the 120°E longitude line but go north across
 170 the 22°N latitude line to the east of Taiwan, then it belongs to a Leap type.
- 171 ● If a streamline intersects the 120°E line twice, which means going in and out
 172 of the SCS, then it belongs to a Loop type.
- 173 ● If a streamline intersects the 120°E line only once, then it is a Leak one.



174

175 Figure 1: Bathymetry of Luzon Strait. The bathymetry data is from Shuttle Radar Topography
176 Mission (SRTM). Two black dot-dash lines are along 120°E and 22°N and used to define
177 streamline types. The blue dash line is defined as an approximate separatrix between the Luzon
178 Strait and the Pacific used to judge whether the streamlines enter or exit the Strait.

179 The choice of 120°E longitude is somewhat subjective. A small shift will only
180 make slight changes of the number of the Loop and Leap types, because there is no
181 clear-cut definition for them by how far the Kuroshio meander reaches. Sometimes
182 only a few streamlines on the outer edge of the flow loop across the 120°E line, while
183 the majority of meanders still stay east of it. By tradition, we would probably call this
184 a loop intrusion, even though the proportion of the loop is very small. In view of this,
185 here we will not be concerned about the intrusion type of the entire Kuroshio but the
186 statistics of the streamline intrusion types instead, e.g. what percentage of streamlines
187 in the Kuroshio take a Leap/Loop/Leak path.

188 Our new algorithm inevitably has difficulty in identifying some streamlines
189 which are apparently unrealistic in physics. For example, some Kuroshio streamlines
190 may just end at the coast of Taiwan or Philippine inside the LS, possibly due to the
191 coarse resolution of the dataset. Our results could also be inadequate to include all
192 Kuroshio streamlines. For instance, there are some intrusion streamlines starting from
193 the northern coast of Philippine. These streamlines might just be misrepresented by
194 the coarse data but should be qualified for the true Kuroshio intrusion in reality. These
195 issues will introduce some uncertainties in our calculation, but the excluded
196 streamlines are expected to occupy only a small proportion and therefore have
197 insignificant influence on the results.

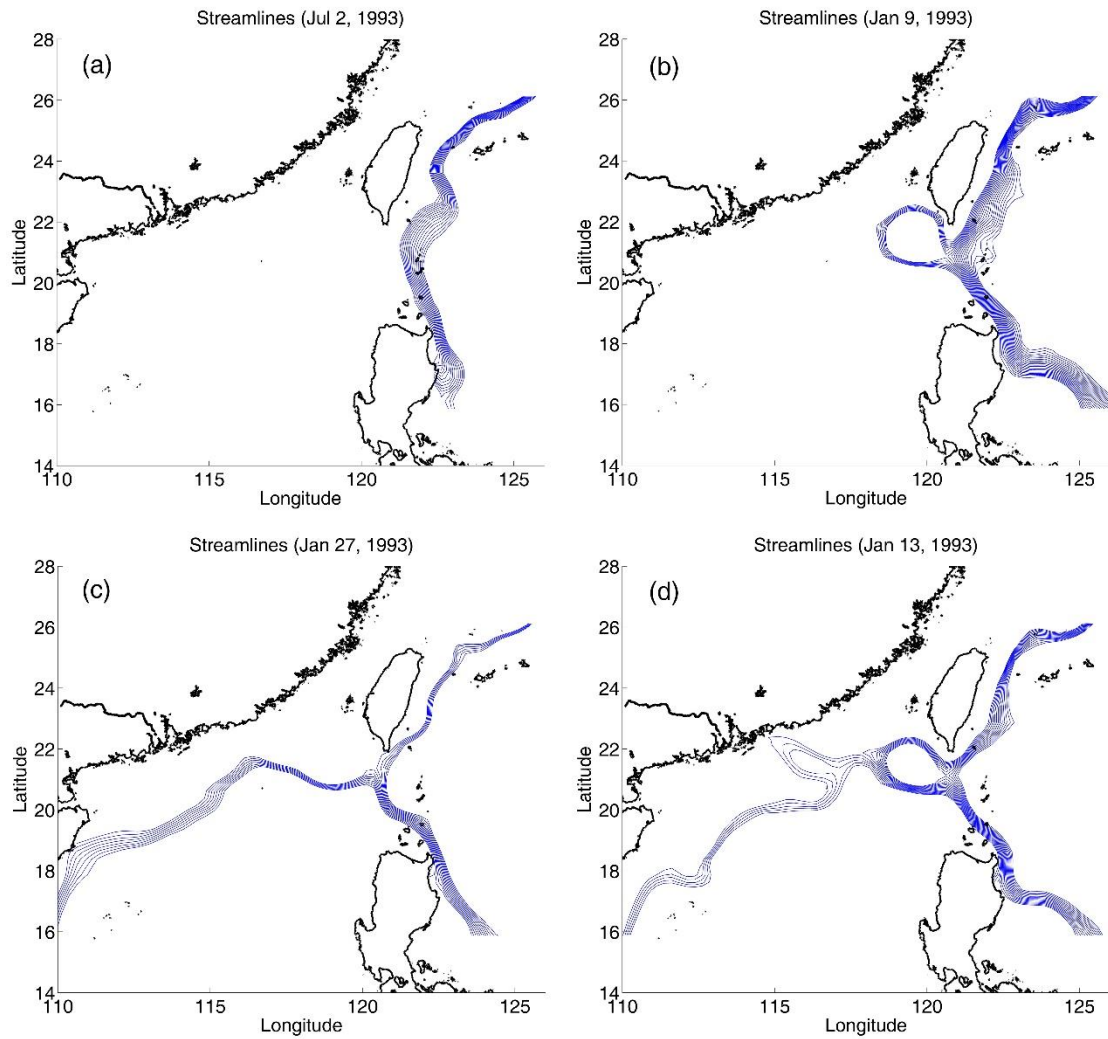
198 **3. Results**

199 **3.1 General statistics of Kuroshio intrusion**

200 Four types of current intrusion are identified using our new method with typical
201 examples demonstrated in Figure 2. Their occurrence frequencies calculated on a

202 daily basis are listed in Table 1. The leaping path accounts for nearly half of the days
203 over the entire 26 years, about 10% higher than the probability presented in Nan et al.
204 (2015). The second most probable scenario is a mixing of all three kinds of
205 streamlines (Leap+Loop+Leak), which contributes nearly one fourth of the total
206 (Fig.2d). This is a new current intrusion type detected using our method. It may be
207 viewed as an intermediate phase between traditional loop and leak intrusion types
208 (Leap+Loop and Leap+Leak streamlines). Interestingly, it turns out that this
209 intermediate type occurs much more frequently than the Loop or Leak types,
210 indicating that the looping and leaking paths are usually not separable, as opposed to
211 that shown in previous classifications. The frequency of the pure loop intrusion is
212 nearly twice as high as that of the leak intrusion, qualitatively in agreement with
213 previous studies.

214 Different current intrusion types also show very strong seasonality (Table 1). The
215 most prominent flow pattern in winter (taking December for an example) is the mixed
216 intrusion type with a nearly half percentage, while in summer (June for example) the
217 Leap type accounts overwhelmingly for more than 90% of the total cases. Note that
218 no Leak type intrusion is detected in June by the algorithm. The Leak streamlines are
219 all within the mixed current type. The rare occurrence of the Leak streamlines is
220 indeed a unique feature of June as shown in the seasonal analysis below. The
221 percentage of each kind of streamline in different current intrusion types is also
222 presented in the Table 1 (inside the parenthesis). The Leap streamlines predominate at
223 all times as expected. Notably it is actually the mixed type that contributes the largest
224 proportion of the net intrusion transport into the SCS. During summer all types of
225 intrusion are extremely weak.



226

227 Figure 2: Examples of four Kuroshio Current intrusion types. (a) Leap; (b) Loop; (c) Leak; (d)

228 Mixed type.

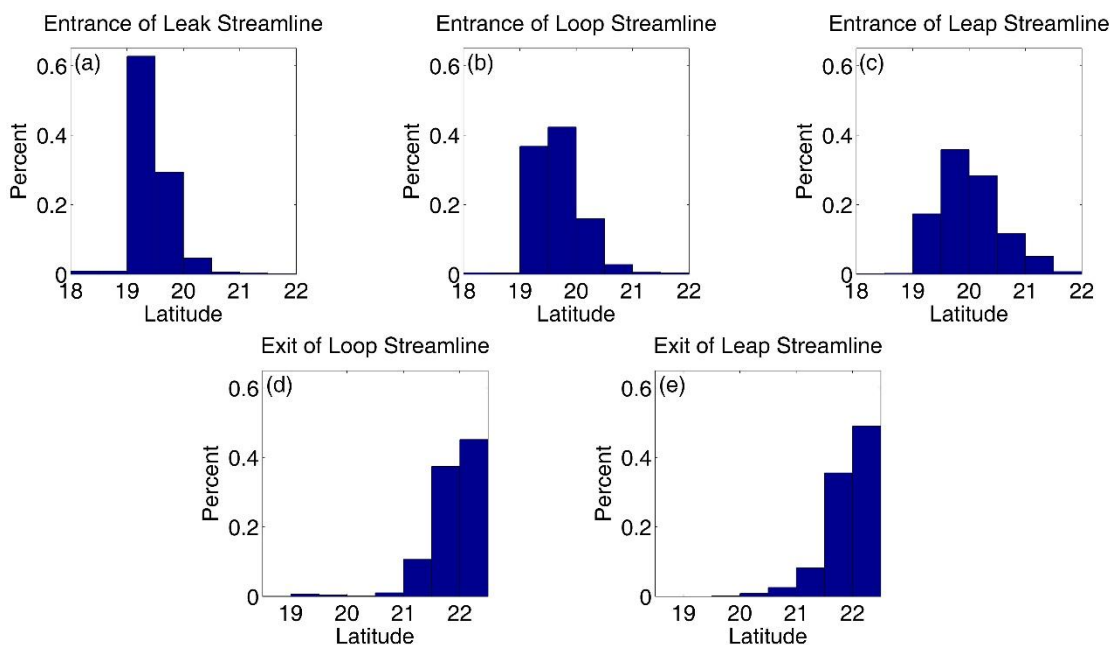
Current intrusion type	Streamline intrusion type	Frequency	Frequency in Dec	Frequency in Jun
Leap	Leap only	49.0% (100%)	9.7% (100%)	91.7% (100%)
Loop	Leap+Loop	17.7% (76.2%+23.8%)	18.2% (57.1%+42.9%)	7.0% (80.7%+19.3%)
Leak	Leap+Leak	10.0% (68.6%+31.4%)	24.4% (61.6%+38.4%)	0% (N/A)
Mixed	Leap+Loop+Leak	23.3% (49.0%+25.2%+25.8%)	47.6% (42.7%+28.4%+28.9%)	1.3% (69.0%+14.0%+17.0%)

229 Table 1: Current intrusion types, Streamline intrusion types and their frequencies over the entire

230 period, in winter and summer respectively. In all frequency columns, the percentage in the

231 parenthesis indicates the percent of each streamline type in the respective current intrusion types.

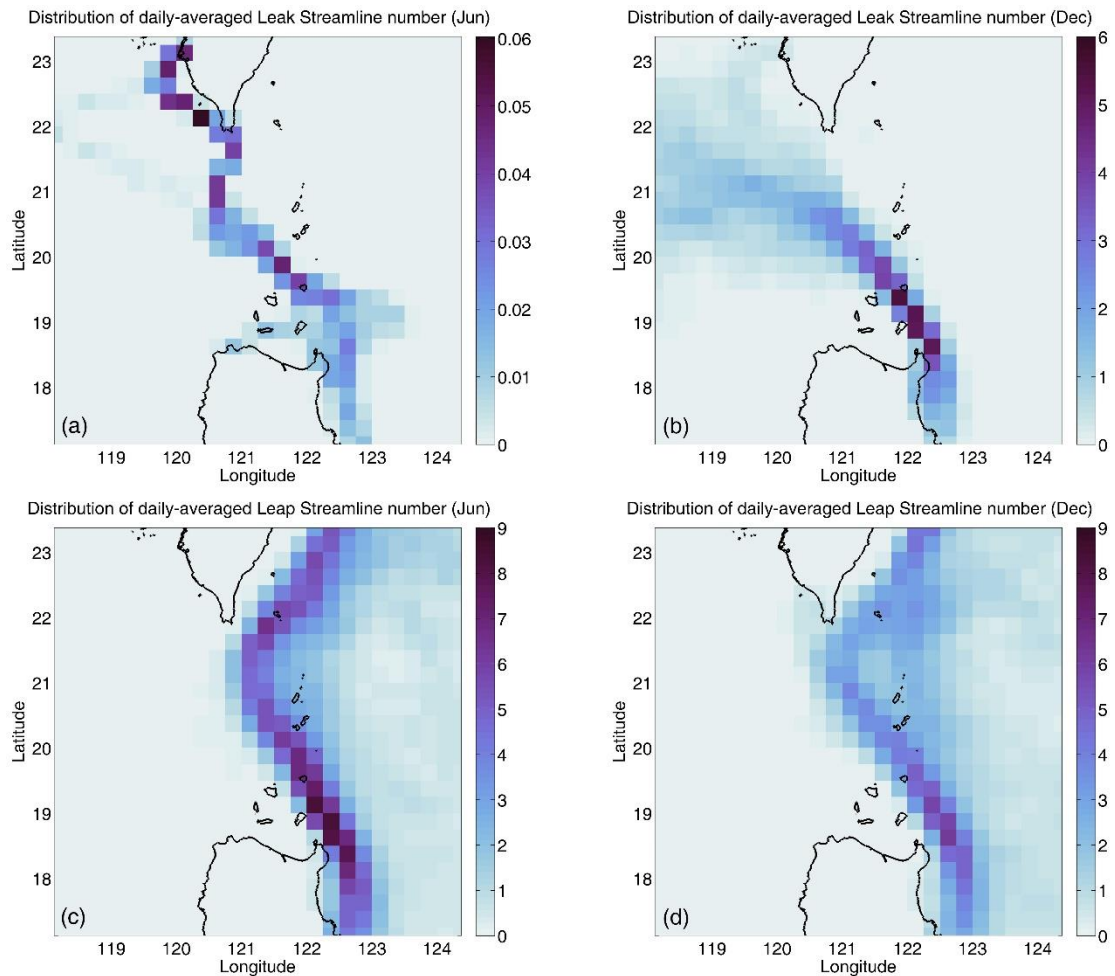
232 A certain amount of the Kuroshio streamlines meanders into the LS all the time,
233 no matter what current intrusion type it is (Figure 2). The traditional viewpoint is that
234 the Kuroshio enters the LS mainly through the Balintang Channel and exit the Strait
235 via the Bashi Channel (e.g. Liang et al., 2003, 2008; Yuan et al., 2008a). Here we
236 define the boundary between the LS and the western Pacific by drawing a straight line
237 roughly along the island chain from the Green Island to the Camiguin Island (blue
238 dash line in Figure 1). With this definition, about 80% of the streamlines intrude into
239 the LS over the entire period. Figure 3 shows that the latitudinal distribution of the
240 entrance for each kind of streamline over the whole period, since it is not quite
241 seasonally dependent. Most of the Leak streamlines intrude into the Strait through the
242 channel between the Babuyan Island and the Camiguin Island (between 19°N and
243 19.5°N), while the Balintang Channel (between 19.5°N and 20.5°N) is the passage
244 most Leap streamlines take. The distribution of the Loop streamlines more or less lies
245 in between. As for the exit latitudes, both of the Loop and Leap streamlines tend to get
246 out of the Strait between 21.5°N and 22.5°N, i.e. the upper half of the Bashi Channel
247 and the channel between the Green Island and the Orchid Island, and the latter seems
248 to have a slightly larger proportion (Fig.3d, e).



249

250 Figure 3: The entrance and exit latitudes of each type of streamlines over the entire period.

251 Figure 4 calculates the daily-averaged number of different streamlines binned
252 onto a $0.25^\circ \times 0.25^\circ$ grid in June and December. Given that the loop intrusion can be
253 seen as an intermediate state between the penetrating and the leaping regime, in the
254 subsequent discussion we will focus on the Leak and Leap streamlines only in June
255 and December, the months with the maximum leaping and the maximum intrusion
256 respectively in a seasonal cycle. The path of the Leap streamlines looks quite stable
257 and independent of any external seasonal forcing (Fig 4c, d). The winter Leak
258 streamlines can generally extend further westwards and their routes are subjected to a
259 large variance once the streamlines are out of the Strait. In summer, the very small
260 number of intrusion streamlines tends to move northwards and end up at the coast. In
261 spite of this unrealistic ending, the direction of the flow could be plausible, possibly
262 due to the steering effect by seasonally-reversing monsoon.



263

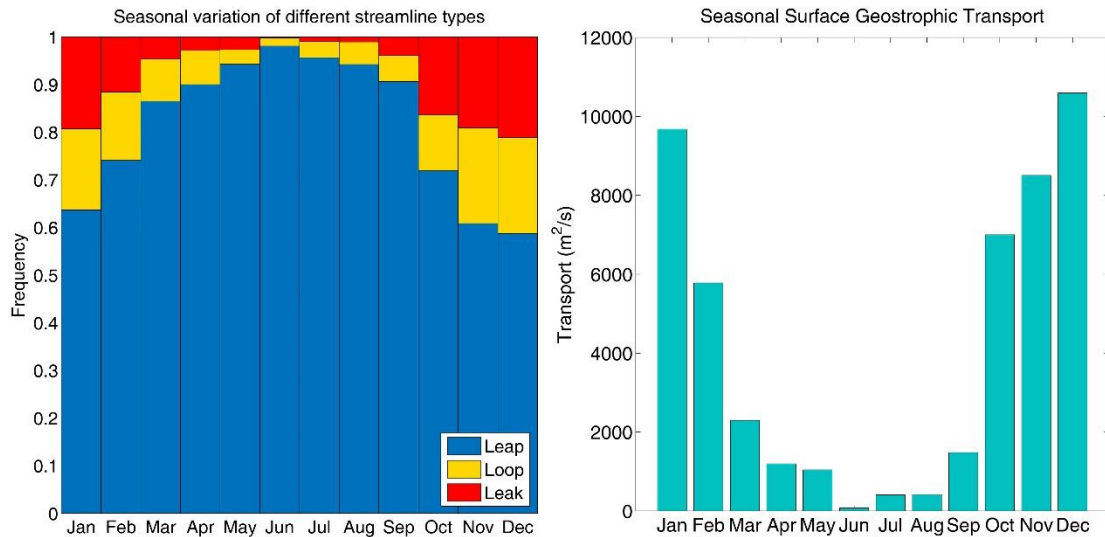
264 Figure 4: The average streamline number binned onto a 0.25×0.25 grid. Note the large difference
 265 in color range.

266 3.2 Seasonal variation of Kuroshio intrusion

267 The characteristics of the seasonal variation of Kuroshio intrusion have been
 268 well documented in a large volume of studies from both observational data and
 269 numerical modeling results. Unlike the general classifications of the flow pattern in
 270 previous works, the results presented here provide a different measure from
 271 streamline perspective. Figure 5 shows the seasonal percentages of each type of
 272 streamline. The advantage of this statistics is that it can more accurately reflect both
 273 the amount and the variation of different flow behaviors. The dominant Leap type
 274 varies between around 60% in winter and over 95% in summer. The Leak streamline
 275 reaches the maximum over 20% in December and reduces to a negligible value in

276 June. Though there is a large probability of intrusion in winter (Nan et al., 2015), the
277 actual Leak streamlines only account for a small portion of the total Kuroshio. The
278 Loop intrusion has nearly the same proportion as the Leak in winter and retains only a
279 small amount in summer. In addition, not all of the streamlines that leak into the SCS
280 will flow westwards and impact the slope current of the northern SCS. The percentage
281 of the along-slope intrusion streamlines has a similar variation on both seasonal and
282 interannual scales (not shown). In terms of the intrusion into the LS as defined in
283 Section 3.1, the seasonal variability is the same but weaker, with the intrusion
284 percentage ranging between 16% in winter and 24% in summer.

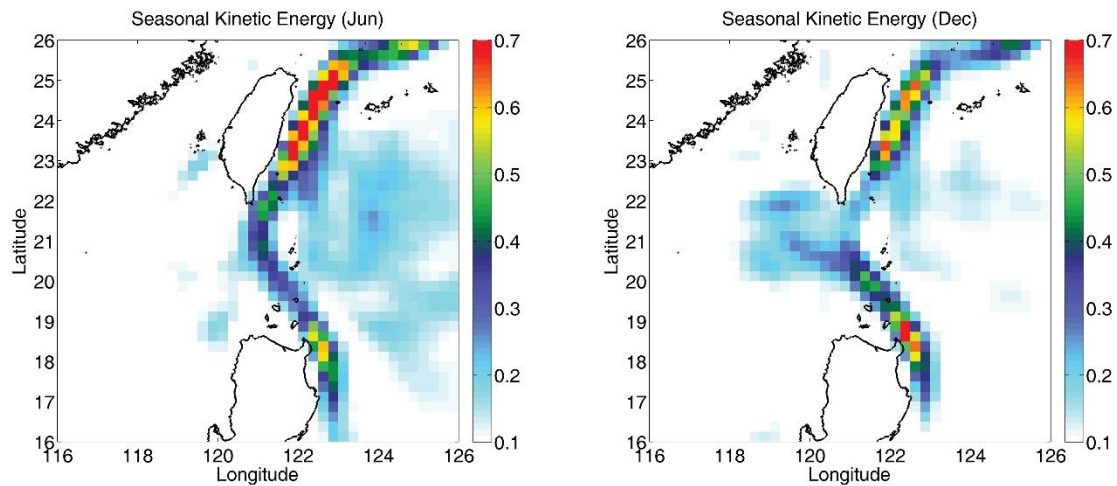
285 The surface geostrophic transport is calculated by accumulating the value
286 differences of adjacent stream functions from Equation (1). The magnitude of the
287 mean surface transport is roughly the same as that given in Qu et al. (2004), but
288 subject to large standard deviations particularly in winter. According to Song (2006),
289 the westward LST above 1500 m can be estimated by the geostrophic flow. Here
290 assuming an upper 1500 m transport with the vertical distribution having an e-folding
291 depth scale of 500 m, the estimated total transport is approximately varying from 0.03
292 to 5.0 Sv seasonally. These very rough estimates are in a reasonable range referring to
293 the in-situ measurements and numerical outputs (Table 1 in Nan et al., 2015). Many
294 studies suggest that during some months of a year the net LST reverses from the SCS
295 to the Pacific (Xue et al., 2004; Yang et al., 2010). Since we only track the Kuroshio
296 streamlines, the results here only account for the westward intrusion from Kuroshio,
297 not the total LST.



298

299 Figure 5: Seasonal variation of the occurrence frequency for the three types of streamlines over
 300 the entire period (left); Seasonal surface intrusion geostrophic transport estimated based on the
 301 Leak streamline number (Right).

302 The seasonality of the Kuroshio Current axis position is also examined along
 303 $18^{\circ}N$ by two different methods. The first one is based on the maximum density of
 304 streamlines, i.e. maximum velocity, and the other uses the longitude where the
 305 zero-vorticity line is located. Both methods estimate the current axis around 50 km
 306 away from the coast with nearly invisible seasonal difference (~ 5 km). Figure 6
 307 shows the seasonal kinetic energy distribution in June and December. The width and
 308 intensity of Kuroshio before turning round into the Strait make slight difference
 309 between the months, and so does the surface transport (Chang & Oey, 2011). The
 310 geostrophic flow is accelerated at the turning corner probably because a larger
 311 pressure gradient is needed to offset the extra centrifugal force. In winter the Kuroshio
 312 has more intrusion streamlines, so the curvature is slightly larger, while in summer the
 313 streamlines primarily belong to the Leap type, leading to a weaker acceleration
 314 associated with the smaller curvature (Fig.3).



315

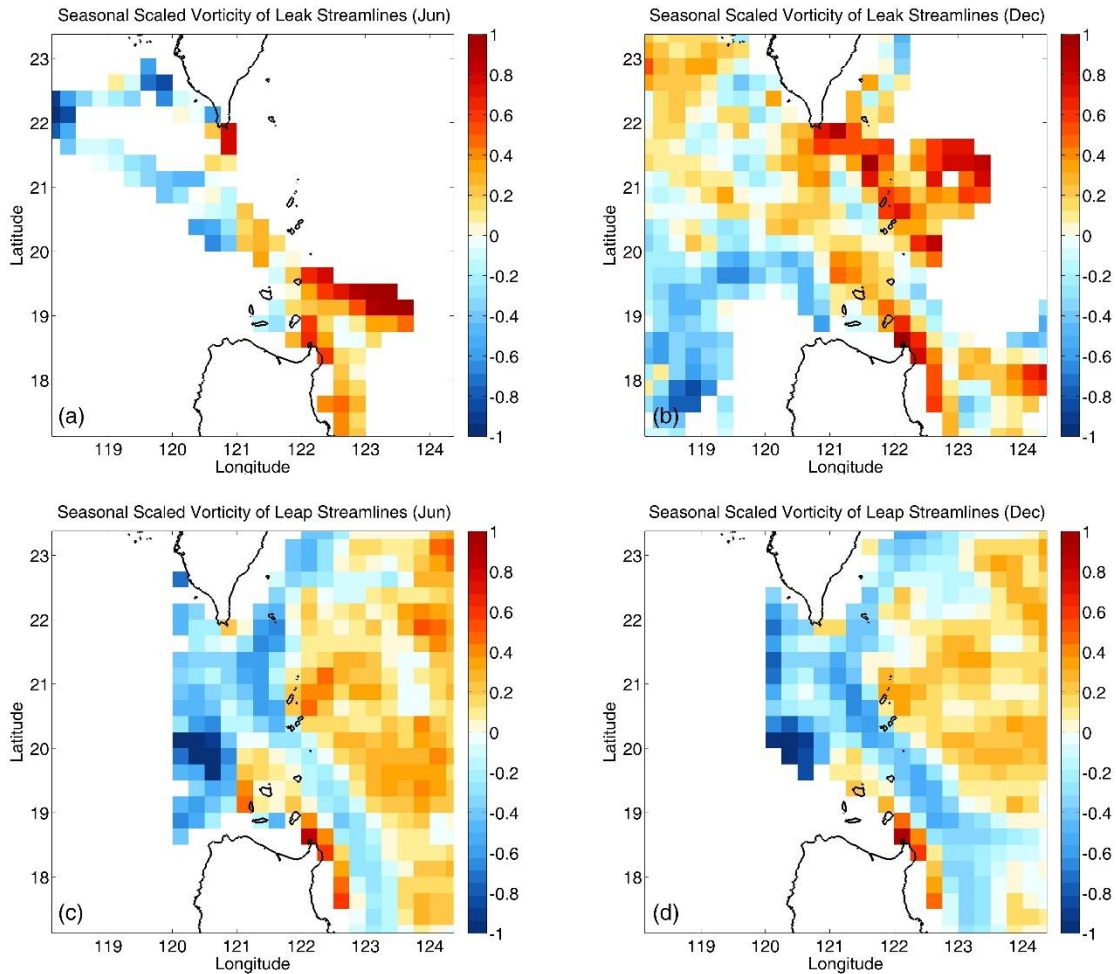
316 Figure 6: Seasonal kinetic energy in June (left) and December (right). Unit: m^2/s^2 .

317 3.3 Dynamical mechanism from streamline analysis

318 3.3.1 Role of lateral velocity shears

319 The streamline-based classification of the Kuroshio inflow regime is
 320 advantageous to distinguishing the characteristics of different streamline types, and
 321 thus provides some new insights into the intrusion mechanisms. Figure 7
 322 demonstrates the bin-averaged vorticity of the Leak and Leap streamlines in June and
 323 December respectively. It is very conspicuous that the majority of the Leak
 324 streamlines have positive vorticity while most Leap streamlines keep negative
 325 vorticity on the way north. The negative magnitudes of the Leap streamlines are about
 326 the same between seasons, in line with the transport variation (Fig.6). In winter, the
 327 strong intrusion can bring the positive vorticity into the SCS. The clear separation
 328 between different streamlines and vorticity polarity is obviously linked with the
 329 horizontal velocity shears. The outer half part of the Kuroshio streamlines, accounting
 330 for about 55% of the total in winter (deduced from Table 1), always leap across the LS
 331 under the influence of their anticyclonic velocity shear, whether it is in summer or
 332 winter. That is to say, the seasonal variation of the Kuroshio intrusion is merely the
 333 variation of the inner part of the flow, i.e., the part with cyclonic velocity shear. The
 334 pattern of the loop case looks more or less like that of the leap in winter (not shown).
 335 In summer the Loop streamlines are too few to draw statistically significant

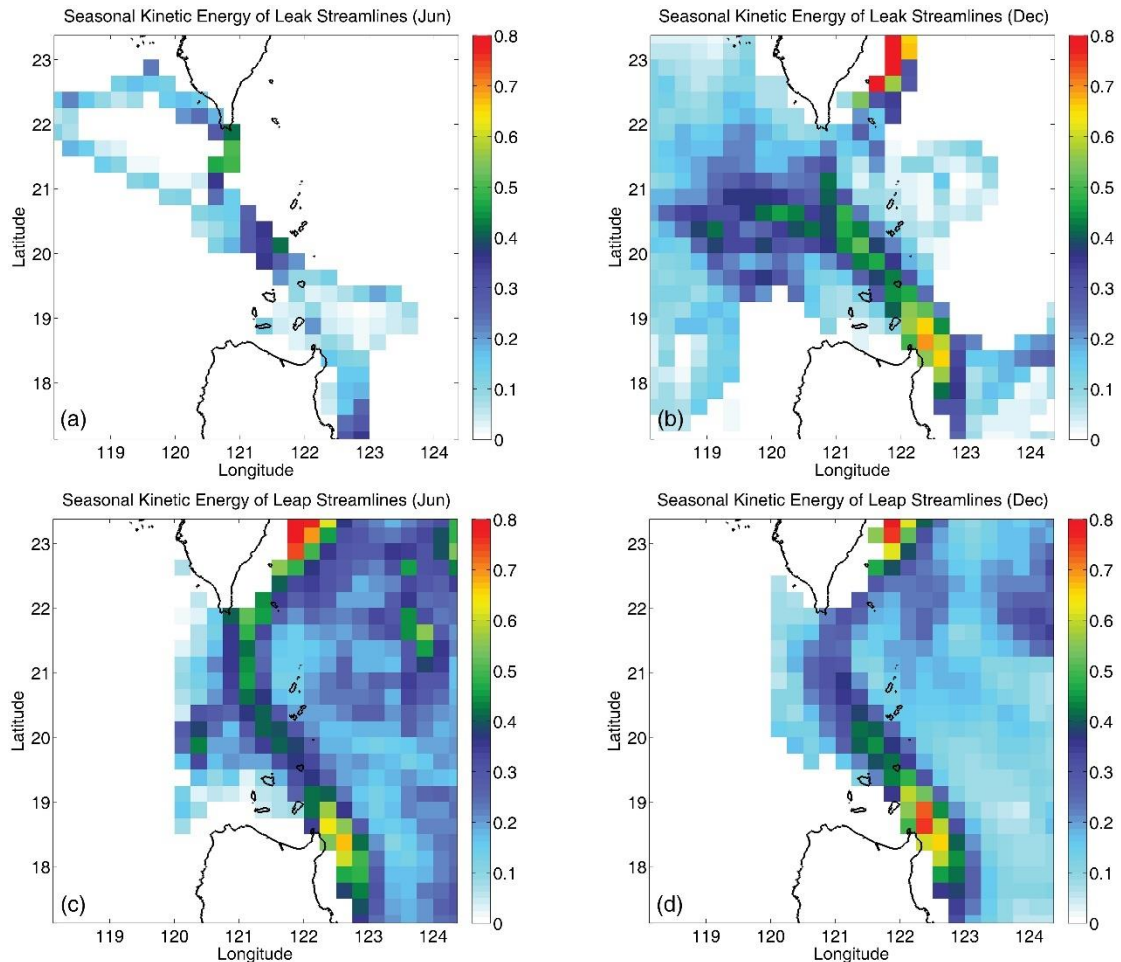
336 conclusions like the Leak ones.



337

338 Figure 7: Seasonal relative vorticity of Leak and Leap streamlines in June and December. The
339 vorticity is nondimensionalized by f .

340 The kinetic energy reduces to some degree along the streamlines, as the
341 streamlines spread out after the jet inflow loses contact with the wall boundary (Fig.8).
342 It is interesting to note that the kinetic energy is not divided half-and-half in
343 December when the current bifurcates in the LS (Fig. 8b, d). Less energy is carried
344 with the Leap streamlines, even they account for 55% of the total. This uneven energy
345 distribution implies a larger portion of kinetic energy possessed by the positive
346 vorticity part of the current in winter. In summer the Leap streamlines have a higher
347 energy level for very few intrusions occur during this season.



348

349 Figure 8: Seasonal kinetic energy of Leak and Leap streamlines. (Unit: m^2/s^2)

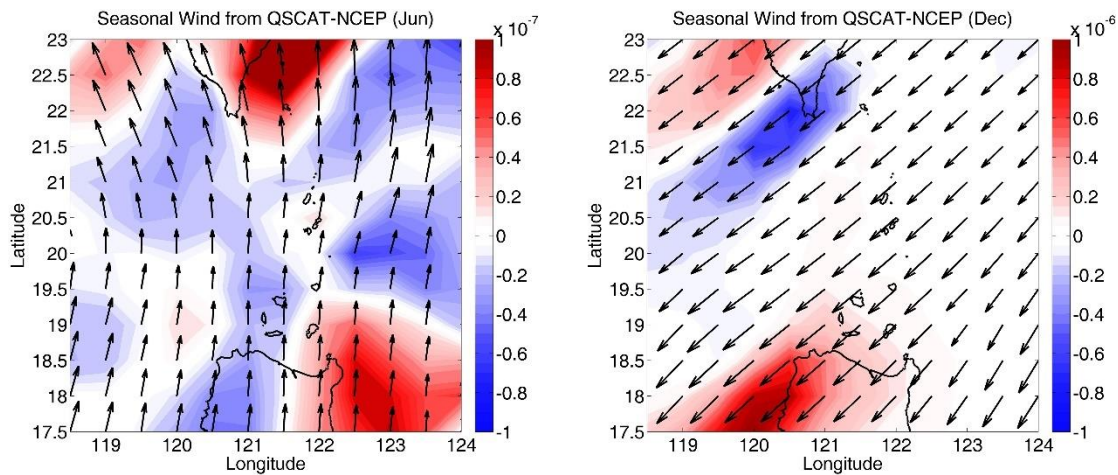
350 **3.3.2 Influences of seasonal monsoon**

351 Given the geostrophic streamlines used in this study, the effect of direct Ekman
 352 transport is naturally ruled out. Nevertheless, winds can still be at play by lifting or
 353 depressing the sea surface level near the lateral boundary or by the stress curl as a
 354 vorticity forcing. By a quick check of historical hydrographic profiles, the
 355 deformation radius is approximately 10 km, limited to a narrow strip along the coast.
 356 However, the current axis in all seasons is close enough to the coast so that a
 357 considerable portion of the cyclonic shear part of the upstream current shall be largely
 358 influenced by the wind. Owing to the coarse resolution of the altimeter data, the
 359 numerical computation of the velocity difference is not accurate enough, so only
 360 qualitative conclusions about this effect may be inferred here. The northeasterly

361 monsoon in winter would pile up the water near the coast, which may reduce the
362 Kuroshio intensity by flattening the surface slope and/or even induce a southward
363 longshore current. Either of them or their combination can increase the cyclonic
364 velocity shear within the boundary layer of the current. The opposite occurs in
365 summer with a weakened lateral velocity shear. This speculation seems reasonable
366 because the seasonal variation of positive vorticity fluxes into the western boundary
367 layer associated with the cyclonic shears have to balance the seasonality of the
368 basin-wide negative wind stress curl, according to the classical wind-driven
369 circulation theory. In addition, given the position, intensity and surface transport of
370 the Kuroshio show little seasonality, this process is practically left to be the only
371 candidate to balance the seasonal wind stress curl input.

372 The seasonal wind stress curls over the intrusion region are shown in Figure 9.
373 The wind product is obtained from QuikSCAT-NCEP blended dataset (Milliff et al.,
374 2004; Northwest Research Associates/Inc., 2001). The scatterometer measures the winds
375 relative to the current, which seems more reliable in the strong current region (Plagge
376 et al., 2012). A notable feature in winter is that extremely large stress curls only occur
377 southwest of Taiwan and northeast of Philippine, while the magnitude in the Pacific
378 sector is nearly an order smaller, very much like that in summer (Fig.9). Over the
379 upstream Kuroshio region ahead of intrusion, the mean vorticity change rate
380 calculated from satellite data is typically of the order of $10^{-9} \sim 10^{-7} \text{ s}^{-2}$ depending on the
381 season. The vorticity contribution from the wind is estimated to be 10^{-10} s^{-2} even for
382 the strong curl regions. Such a weak stress curl is thus expected to have a negligible
383 impact on the mixed layer vorticity budget, in agreement with the vorticity analysis
384 results from Nan et al. (2011a). Wu and Hsin (2012) presents the negative curl off
385 southwest Taiwan is strongly correlated with the depth-averaged kinetic energy in the
386 center of Luzon Strait, suggesting that the wind curl can help the Kuroshio intrusion
387 into the SCS. In this study with the surface streamlines we only attempt to investigate
388 the link between the intensity of this curl and the surface intrusion probability, i.e., the
389 total percentage of the Leak and Loop streamlines. The correlation between them

390 turns out to be very weak (below 0.4). Since the satellite data limit our analysis to the
391 surface only, no further exploration can be done on how this discrepancy comes
392 about.



393

394 Figure 9: Seasonal wind vectors and wind stress curls (shaded, Unit: N/m^3) derived from
395 QSCAT-NCEP blended wind in June (left) and December (right). Note that the magnitude is an
396 order difference between the two panels.

397 3.3.3 A possible mechanism for Kuroshio intrusion

398 In light of the weak seasonality of the Kuroshio intensity, position and width, the
399 strong seasonal cycle of the geostrophic Kuroshio intrusion poses a question in
400 explaining the controlling mechanism behind, which the theories reviewed in Section
401 1 cannot well address. In this section we attempt to seek a suitable interpretation to
402 accommodate all the seasonal characteristics of Kuroshio intrusion discussed above.
403 In particular, the divergence of streamlines with positive and negative vorticities shed
404 some light on what determines the current to leap across or leak into the Strait.
405 However, the data resolution is so coarse that the western boundary current is covered
406 by only a few grid points (Fig.6). Any numerical computation on high-order
407 derivatives could cause unanticipated errors in such a dynamic region. As a
408 consequence, we will have to conjecture the mechanism of Kuroshio intrusion to a
409 certain extent based on classical theories. We shall consider this issue from a “global”

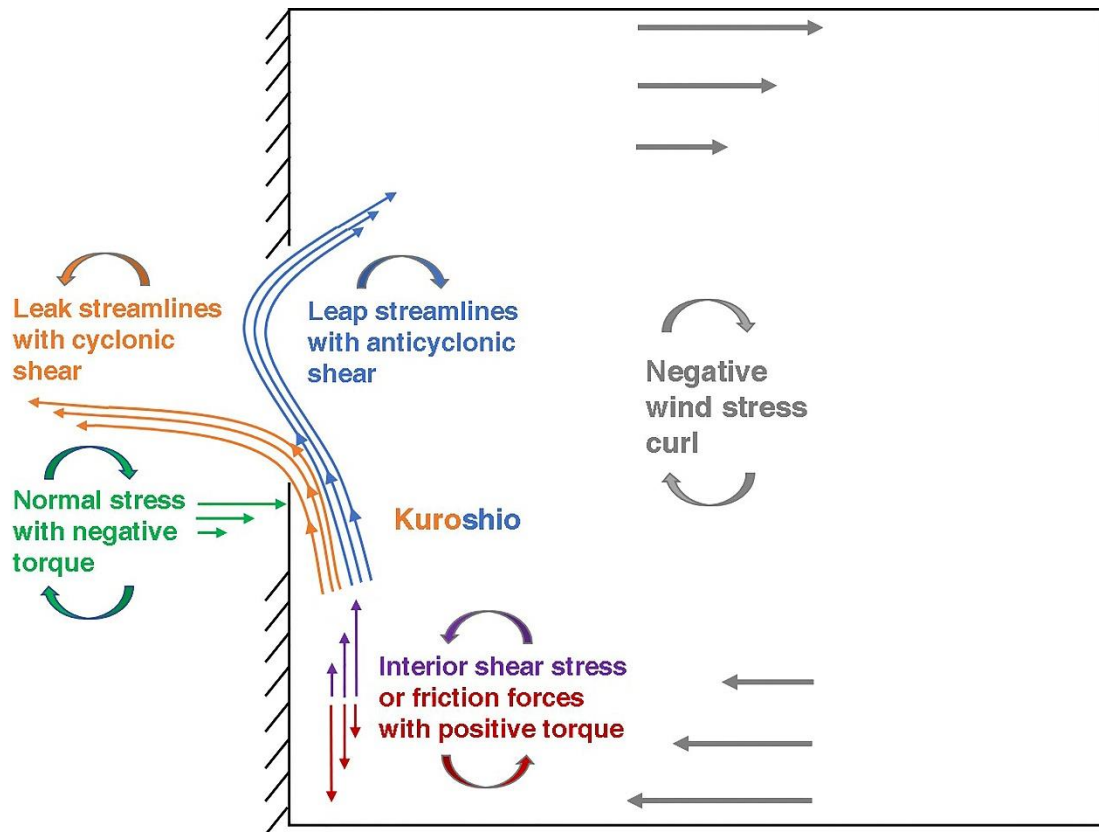
410 and a “local” perspective (Figure 10).

411 From a “global” view, the basin-wide negative wind curls drive an anticyclonic
412 circulation with negative vorticity (anticyclonic velocity shear). In other words, the
413 anticyclonic velocity shear of the current reflects the anticyclonic flow tendency in
414 response to the negative wind curl forcing. A counteracting effect is required to brake
415 the current and maintain the vorticity balance or the torque balance with the wind
416 forces. This work can be done by the lateral friction force according to Munk’s theory
417 (Munk, 1950), which dissipates the flow energy and induces cyclonic shears of the
418 boundary current by imposing a positive torque. The anticyclonic shear part of the
419 flow always has a tendency to lead the current northward to close up the anticyclonic
420 gyre, whether there is a gap on the western boundary or not. Stated from the vorticity
421 perspective, the positive vorticity fluxes into the western boundary flow at each
422 latitude are exactly in balance with the negative vorticity inputs by wind stress
423 (Pedlosky, 2010). Once the flow encounters a boundary gap, the positive vorticity
424 source is shut down and the unbalanced negative vorticity associated with the
425 anticyclonic velocity shear would drive the current northward to a place with higher
426 ambient vorticity.

427 The “local” view zooms into the western boundary region, where the cyclonic
428 friction torque imposed by the wall must be locally balanced to keep the flow steady.
429 The local wind stress curls have been seen to be too weak to counteract this torque
430 (Fig.9). As a matter of fact, it is the torque of the normal stresses exerted by the wall
431 boundary that provide such a counteracting effect. An analog in rigid body dynamics
432 is that if a solid cube is pushed forwards on a frictional surface, the torque of friction
433 forces must be balanced by the torque of normal forces to prevent the cube from
434 rolling over. In the fluid case here, the non-uniform normal stresses generate a
435 negative torque against the friction stresses to keep the current parallel to the
436 boundary (red and green arrows in Fig. 10). It is worthwhile to clarify the difference
437 from the wind-friction torque balance discussed in the “global” view. The torque of

438 normal stresses doesn't do any work because no displacement perpendicular to the
439 boundary is allowed. For this reason, the aforementioned wind-friction torque balance
440 should be stated more exactly as the balance between the work done by the wind
441 stress torque and by the friction stress torque along the western boundary. The
442 vorticity is produced by the torque work, so the vorticity balance should involve only
443 the wind and the friction effects. When the boundary current encounters a gap, it
444 immediately loses the normal stress torque and is bent into the gap by the positive
445 torque of interior shear stresses left by the lateral friction. The interior shear stress is
446 usually parameterized in the form of $A_H \partial^2 v / \partial x^2$. A very loose calculation using
447 satellite data shows it is indeed positive for the entire current in line with Munk's
448 solution. This explains why most of Kuroshio streamlines always meander through
449 the LS (Fig. 2). It is also the hydrodynamic interpretation of the "teapot effect"
450 (Kistler & Scriven, 1994).

451 Based on the "global" and "local" viewpoints, we see that there is a competition
452 in the Kuroshio Current between a cyclonic tendency of movement due to the local
453 unbalanced positive torque of interior shear stresses and an anticyclonic tendency of
454 movement due to the global negative vorticity forcing of wind stresses. The kinematic
455 structures of the Kuroshio are very similar over all seasons except a coastal strip
456 where the cyclonic velocity shear might be significantly modified by the
457 seasonally-reversing monsoon. Therefore, the Leap streamlines, located mostly on the
458 outer part of the flow, are always prone to flow anticyclonically following a stable
459 path regardless of seasons (Fig.3 and 4). In contrast, the inner part of the flow is
460 largely influenced by the seasonally-varying cyclonic velocity shears. In summer, the
461 monsoon-induced longshore current may weaken the interior stress torque, which is
462 then not able to resist the anticyclonic tendency, therefore the entire current leaps
463 across the Strait. On the contrary, the cyclonic interior stress torque is strengthened by
464 the monsoon in winter so that this portion of the streamlines is torn apart from the
465 main stream and intrude westwards into the SCS.



466

467 Figure 10: Sketch of the 'global' and 'local' views of Kuroshio intrusion

468 **4. Discussion and conclusions**

469 We have developed a streamline-based algorithm to identify the intrusion types
 470 and make a thorough investigation on the seasonality of a number of Kuroshio
 471 intrusion properties using satellite altimeter data. Unlike the results from previous
 472 identification methods, it turns out that a mixed type with all kinds of streamlines is
 473 the dominant flow pattern in winter. The streamline entrance locations into the LS
 474 vary depending only on the streamline types, and the intensity, width and current axis
 475 of the Kuroshio also show insignificant seasonal variabilities. The use of geostrophic
 476 velocities precludes the direct Ekman transport effect, and the magnitude of local
 477 wind stress curls is too small to influence the upstream Kuroshio into the LS.

478 In light of all these characteristics, it appears that none of the physical
 479 mechanisms proposed by preceding studies could fully explain the seasonal intrusion
 480 variability. Noting a clear partition between the Leak streamlines with cyclonic

481 velocity shears and the Leap streamlines with anticyclonic shears, we present a new
482 interpretation based on globally the vorticity balance (torque work balance) between
483 negative wind curl input and positive frictionally-induced vorticity fluxes, and locally
484 the loss of balance between the interior stress torque and the normal stress torque both
485 provided by the wall boundary. Due to the coarse resolution of satellite data, a
486 conjecture has to be made that the seasonally-reversing monsoon would significantly
487 modify the cyclonic velocity shears in the inner part of the Kuroshio, leading to the
488 seasonal variations of the interior stress torque and thus the Kuroshio intrusion. Given
489 that the basin-wide wind curl is also seasonally-varying, which must be balanced by
490 frictionally-induced vorticity, we anticipate that this conjecture should be reasonable.

491 The physical interpretation we discussed above attributes the seasonal variation
492 of Kuroshio intrusion to a single external factor — the local monsoon and a series of
493 dynamical processes. It doesn't mean that other factors have no influence on the
494 intrusion, but that the monsoon merely stands out under some certain kinetic
495 conditions of Kuroshio on the seasonal scale. For example, we also anticipate that the
496 current inertia characterized by Reynolds number $Re = Q/A_H$ is an important factor
497 (Sheremet 2001), though the Kuroshio transport Q is roughly invariant on the
498 seasonal scale. On an interannual scale, the shift of the north equatorial current
499 bifurcation may change the Kuroshio transport and further affect the Kuroshio
500 intrusion (e.g. Kim et al., 2004). Sheremet (2001) also shows the occurrence of
501 hysteresis in the flow evolution, which is considered to be averaged out over a
502 seasonal time scale. The direct Ekman effect by the monsoon could be also important
503 to enhance the intrusion in the LS (Wu & Hsin, 2012), but our method is unable to
504 evaluate its contribution.

505 One possible issue with satellite-derived streamlines is that the geostrophic
506 current may not well represent the true current, especially within the boundary layer
507 where the lateral friction is a significant term in the momentum balance. In addition,
508 the lateral friction could also be important to the wind setup of surface elevations near

509 the coast. High-resolution nearshore in-situ measurements or numerical simulations
510 with a proper parameterization are needed to examine the role of the lateral friction
511 and corroborate the theory discussed above. One may also argue that the streamlines
512 are in Eulerian but not Lagrangian framework. The typical magnitude of absolute
513 dynamical height is 1 m while its daily variation is of the order of 10^{-2} m over the
514 intrusion region. With the intrusion path of 300 km and the current speed of 0.6m/s,
515 we get a time scale of about 6 days. So, it should be safe to assume the flow is
516 approximately stationary over a full period of Kuroshio intrusion.

517 **5. Acknowledgements**

518 The altimeter data provided by E. U. Copernicus Marine Service Information is
519 downloaded from
520 [http://marine.copernicus.eu/services-portfolio/access-to-products/?option=com_csw&](http://marine.copernicus.eu/services-portfolio/access-to-products/?option=com_csw&view=details&product_id=SEALEVEL_GLO_PHY_CLIMATE_L4_REP_OBSERVATIONS_008_057)
521 [view=details&product_id=SEALEVEL_GLO_PHY_CLIMATE_L4_REP_OBSERVA](http://marine.copernicus.eu/services-portfolio/access-to-products/?option=com_csw&view=details&product_id=SEALEVEL_GLO_PHY_CLIMATE_L4_REP_OBSERVATIONS_008_057)
522 [TIONS_008_057](http://marine.copernicus.eu/services-portfolio/access-to-products/?option=com_csw&view=details&product_id=SEALEVEL_GLO_PHY_CLIMATE_L4_REP_OBSERVATIONS_008_057). The QSCAT-NCEP blended dataset is obtained from
523 <https://rda.ucar.edu/datasets/ds744.4>. The data products are properly cited and referred
524 in the reference list. This work is supported by the grants from the National Natural
525 Science Foundation of China (No. 41706014), the Sino-German Cooperation in ocean
526 and polar research – Megacity’s fingerprint in Chinese marginal seas: Pollutant
527 fingerprints and dispersal transformation (MEGAPOL), the International Cooperation
528 of the National Natural Science Foundation of China (No. 41861134040) and the
529 National Program on Key Basic Research Project of China (973 Program, No.
530 2014CB441500). J.W. is supported by MEGAPOL with the contract number to
531 it BMBf (03F0786A) Federal Ministry of Education and Research and
532 SOCLIS-SO269 FKZ 03G0269. L.Z. is supported by the National Natural Science
533 Foundation of China (No. 41690121, 41690120, 41530961)

534 **References**

535 Caruso, M. J., Gawwarkiewicz, G. G. & Beardsley, R. C. (2006). Interannual variability of the
536 Kuroshio intrusion in the South China Sea. *Journal of Oceanography*, 62, 559–575.

- 537 [https://doi.org/ 10.1007/s10872-006-0076-0](https://doi.org/10.1007/s10872-006-0076-0).
- 538 Chang, Y.-L. & Oey, L.-Y. (2011). Interannual and seasonal variations of Kuroshio transport east
539 of Taiwan inferred from 29 years of tide-gauge data. *Geophysical Research Letters*, 38,
540 L08603. <https://doi.org/10.1029/2011GL047062>.
- 541 Chen, Y., Zhai, F. & Li, P. (2020). Decadal variation of the Kuroshio intrusion into the South
542 China Sea During 1992-2016. *Journal of Geophysical Research*, 125, e2019JC015699.
543 <https://doi.org/10.1029/2019JC015699>.
- 544 Farris, A. & Wimbush, M. (1996). Wind-induced Kuroshio intrusion into the South China Sea.
545 *Journal of Oceanography*, 52, 771–784. <https://doi.org/10.1007/BF02239465>.
- 546 Hsin, Y.-C., Wu, C.-R. & Chao, S.-Y. (2012). An updated examination of the Luzon Strait
547 transport. *Journal of Geophysical Research*, 117, C03022.
548 <https://doi.org/10.1029/2011JC007714>.
- 549 Kim, Y.Y., Qu, T., Jensen, T., Miyama, T., Mitsudera, H., Kang, H.-W. & Ishida, A. (2004).
550 Seasonal and interannual variations of the North Equatorial Current bifurcation in a
551 high-resolution OGCM. *Journal of Geophysical Research*, 109, C03040.
552 <https://doi.org/10.1029/2003JC002013>.
- 553 Kistler, S. F. & Scriven, L. E. (1994). The teapot effect: Sheet-forming flows with deflection,
554 wetting and hysteresis. *Journal of Fluid Mechanics*, 263, 19–62.
555 <https://doi.org/10.1017/S0022112094004027>.
- 556 Kuehl, J. J. & Sheremet, V. A. (2009). Identification of a cusp catastrophe in a gap-leaping
557 western boundary current. *Journal of Marine Research*, 67, 25–42.
558 <https://doi.org/10.1357/002224009788597908>
- 559 Lan, J., Bao, X. & Gao, G. (2004). Optimal estimation of zonal velocity and transport through
560 Luzon Strait using variational data assimilation technique. *Chinese Journal of Oceanology
561 and Limnology*, 22, 335–339. <https://doi.org/10.1007/BF02843626>.
- 562 Liang, W.-D., Tang, T. Y., Yang, Y. J., Ko, M. T. & Chuang, W.-S. (2003). Upper-ocean currents
563 around Taiwan. *Deep-Sea Research II: Topical Studies in Oceanography*, 50, 1085–1105.
564 [https://doi.org/10.1016/S0967-0645\(03\)00011-0](https://doi.org/10.1016/S0967-0645(03)00011-0).
- 565 Liang, W.-D., Yang, Y.J., Tang, T.Y. & Chuang, W.-S. (2008). Kuroshio in the Luzon Strait.
566 *Journal of Geophysical Research*, 113, C08048. <https://doi.org/10.1029/2007JC004609>.
- 567 Metzger, E. J. & Hurlburt, H. E. (1996). Coupled dynamics of the South China Sea, the Sulu Sea,
568 and the Pacific Ocean. *Journal of Geophysical Research*, 101(C5), 12 331–12352.
569 <https://doi.org/10.1029/95JC03861>.
- 570 Metzger, E. J. & Hurlburt, H. E. (2001). The nondeterministic nature of Kuroshio penetration and

571 eddy shedding in the South China Sea. *Journal of Physical Oceanography*, 31(7), 1712–1732.
572 [https://doi.org/10.1175/1520-0485\(2001\)031<1712:TNNOKP>2.0.CO;2](https://doi.org/10.1175/1520-0485(2001)031<1712:TNNOKP>2.0.CO;2).

573 Milliff, R. F., Morzel, J., Chelton, D. B. & Freilich, M. H. (2004). Wind stress curl and wind
574 stress divergence biases from rain effects on QSCAT surface wind retrievals. *Journal of*
575 *Atmospheric and Oceanic Technology*, 21(8), 1216–1231.
576 [https://doi.org/10.1175/1520-0426\(2004\)021<1216:WSCAWS>2.0.CO;2](https://doi.org/10.1175/1520-0426(2004)021<1216:WSCAWS>2.0.CO;2).

577 Munk, W. H. (1950). On the wind-driven ocean circulation. *Journal of Meteorology*, 7(2), 79–93.
578 [https://doi.org/10.1175/1520-0469\(1950\)007<0080:OTWDOC>2.0.CO;2](https://doi.org/10.1175/1520-0469(1950)007<0080:OTWDOC>2.0.CO;2).

579 Nan, F., Xue, H., Chai, F., Shi, L., Shi, M. & Guo, P. (2011a). Identification of different types of
580 Kuroshio intrusion into the South China Sea. *Ocean Dynamics*, 61, 1291–1304.
581 <https://doi.org/10.1007/s10236-011-0426-3>.

582 Nan, F., Xue, H., Xiu, P., Chai, F., Shi, M. & Guo, P. (2011b). Oceanic eddy formation and
583 propagation southwest of Taiwan. *Journal of Geophysical Research*, 116, C12045.
584 <https://doi.org/10.1029/2011JC007386>.

585 Northwest Research Associates/Inc. (2001), QSCAT/NCEP Blended Ocean Winds from Colorado
586 Research Associates (version 5.0), <https://doi.org/10.5065/XQYC-1602>, Research Data
587 Archive at the National Center for Atmospheric Research, Computational and Information
588 Systems Laboratory, Boulder, Colo. Accessed 9 Apr 2020.

589 Pedlosky, J. (2010). *Ocean Circulation Theory*. Springer Berlin Heidelberg

590 Plagge, A. M., Vandemark, D. & Chapron, B. (2012). Examining the impact of surface currents on
591 satellite scatterometer and altimeter ocean winds. *Journal of Atmospheric and Oceanic*
592 *Technology*, 29(12), 1776–1793. <https://doi.org/10.1175/JTECH-D-12-00017.1>.

593 Qu, T. (2000). Upper-layer circulation in the South China Sea. *Journal of Physical Oceanography*,
594 30(6), 1450–1460. [https://doi.org/10.1175/1520-0485\(2000\)030<1450:ULCITS>2.0.CO;2](https://doi.org/10.1175/1520-0485(2000)030<1450:ULCITS>2.0.CO;2).

595 Qu, T., Kim, Y. Y., Yaremchuk, M., Tozuka, T., Ishida, A. & Yamagata, T. (2004). Can Luzon
596 strait transport play a role in conveying the impact of ENSO to the South China Sea? *Journal*
597 *of Climate*, 17(18), 3644–3657. [https://doi.org/10.1175/1520-0442\(2004\)](https://doi.org/10.1175/1520-0442(2004)017<3644:CLSTPA>2.0.CO;2)
598 [017<3644:CLSTPA>2.0.CO;2](https://doi.org/10.1175/1520-0442(2004)017<3644:CLSTPA>2.0.CO;2).

599 Sheremet, V. A. (2001). Hysteresis of a western boundary current leaping across a gap. *Journal of*
600 *Physical Oceanography*, 31(5), 1247–1259.
601 [https://doi.org/10.1175/1520-0485\(2001\)031<1247:HOAWBC>2.0.CO;2](https://doi.org/10.1175/1520-0485(2001)031<1247:HOAWBC>2.0.CO;2)

602 Sheu, W.-J., Wu, C.-R. & Oey, L.-Y. (2010). Blocking and westward passage of eddies in the
603 Luzon Strait. *Deep-Sea Research II: Topical Studies in Oceanography*, 57, 1783–1791.
604 <https://doi.org/10.1016/j.dsr2.2010.04.004>.

- 605 Song, Y. T. (2006). Estimation of interbasin transport using ocean bottom pressure: theory and
606 model for Asian marginal seas. *Journal of Geophysical Research*, *111*, C11S19.
607 <https://doi.org/10.1029/2005JC003189>.
- 608 Wu, C.-R. (2013). Interannual modulation of the Pacific Decadal Oscillation (PDO) on the
609 low-latitude western North Pacific. *Progress in Oceanography*, *110*, 49–58.
610 <https://doi.org/10.1016/j.pocean.2012.12.001>.
- 611 Wu, C.-R. & Hsin, Y.-C. (2012). The forcing mechanism leading to the Kuroshio intrusion into
612 the South China Sea. *Journal of Geophysical Research*, *117*, C07015.
613 <https://doi.org/10.1029/2012JC007968>.
- 614 Xu, J. P., Shi, M. C., Zhu, B. K. & Liu, Z. H. (2004). Several characteristics of water exchange in
615 the Luzon Strait. *Acta Oceanologica Sinica*, *23* (1), 11–22.
- 616 Xu, J. P. & Su, J. L. (2000). Hydrological analysis of Kuroshio water intrusion into the South
617 China Sea. *Acta Oceanologica Sinica*, *19* (3), 1–21.
- 618 Xue, H. J., Chai, F., Pettigrew, N. R., Xu, D. Y., Shi, M. C. & Xu, J. P. (2004). Kuroshio intrusion
619 and the circulation in the South China Sea. *Journal of Geophysical Research*, *109*, C02017.
620 <https://doi.org/10.1029/2002JC001724>.
- 621 Yang, Q., Tian, J. & Zhao, W. (2010). Observation of Luzon Strait transport in summer 2007.
622 *Deep-Sea Research I: Oceanographic Research Papers*, *57*(5), 670–676.
623 <https://doi.org/10.1016/j.dsr.2010.02.004>.
- 624 Yang, J., Lin, X. & Wu, D. (2013). On the dynamics of the seasonal variation in the South China
625 Sea throughflow transport. *Journal of Geophysical Research Oceans*, *118*(12), 6854–6866.
626 <https://doi.org/10.1002/2013JC009367>.
- 627 Yaremchuk, M. & Qu, T. (2004). Seasonal variability of the large-scale currents near the coast of
628 the Philippines. *Journal of Physical Oceanography*, *34*(4), 844–855. [https://doi.org/
629 10.1175/1520-0485\(2004\)034<0844:SVOTLC>2.0.CO;2](https://doi.org/10.1175/1520-0485(2004)034<0844:SVOTLC>2.0.CO;2).
- 630 Yuan, Y., Liao, G., Guan, W., Wang, H., Lou, R. & Chen, H. (2008). The circulation in the upper
631 and middle layers of the Luzon Strait during spring 2002. *Journal of Geophysical Research*,
632 *113*, C06004. <https://doi.org/10.1029/2007JC004546>.
- 633 Yuan, D. L., Han, W. Q. & Hu, D. X. (2006). Surface Kuroshio path in the Luzon Strait area
634 derived from satellite remote sensing data. *Journal of Geophysical Research*, *111*, C11007.
635 <https://doi.org/10.1029/2005JC003412>.